A Prediction Model that Combines Rain Attenuation and Other Propagation Impairments Along Earth-Satellite Paths

Asoka Dissanayake[1], Jeremy Allnutt[2], Fatim Haidara[3]

Abstract - The rapid growth of satellite services using higher frequency bands such as the Ka-band has highlighted a need for estimating the combined effect of different propagation impairments. Many projected Ka-band services will use very small terminals and, for some, rain effects may only form a relatively small part of the total propagation link margin. It is therefore necessary to identify and predict the overall impact of every significant attenuating effect along any given path. A procedure for predicting the combined effect of rain attenuation and several other propagation impairments along earth-satellite paths is presented. Where accurate model exist for some phenomena, these have been incorporated into the prediction procedure. New models were developed, however, for rain attenuation, cloud attenuation, and low-angle fading to provide more overall accuracy, particularly at very low elevation angles ($<10°$). In the absence of a detailed knowledge of the occurrence probabilities of different impairments, an empirical approach is taken in estimating their combined effects. An evaluation of the procedure is made using slant-path attenuation data that have been collected with simultaneous beacon and radiometer measurements which allow a near complete account of different impairments. Results indicate that the rain attenuation element of the model provides the best average accuracy globally between 10 and 30 GHz and that the combined procedure gives prediction accuracies comparable to uncertainties associated with the year-to-year variability of path attenuation.

Index Terms - Microwave radio propagation meteorological factors, Satellite communication.

I. INTRODUCTION

Rapid growth in new satellite services incorporating Very Small Aperture Terminals (VSAT) and Ultra Small Aperture Terminals (USAT) is expected in the coming years. Small size terminals allow for widespread use of satellite services in small business and domestic applications. Some of the services that can benefit from small

[1]COMSAT Laboaratories, 2300 COMSAT Drive, Clarksburg, MD 20871
[2]VPI&SU, Northern Virginia Graduate Center, 7054 Haycock Road, Falls Church, VA 22043-2311
[3]INTELSAT, 3400 International Drive, NW Washington DC 20008

earth terminals include: Internet access, multimedia applications, Local Area Network (LAN) interconnection, Supervisory Control and Data Acquisition (SCADA) and point of sales verification. Due to congestion of lower frequency bands such as C and Ku, most of these services will use Ka-band (20/30 GHz) frequencies.   Propagation impairments produced by the troposphere are a limiting factor for the effective use of the 20/30 GHz band and the use of smaller earth terminals*, while very attractive for customer premise location, makes it difficult to provide sufficient link margins for propagation related outages. In this context, reliable prediction of propagation impairments for low-margin systems becomes important. This paper reports a methodology that will allow the prediction of different types of propagation impairments as well as combining them together to determine the overall impact on satellite links over a wide range of outage probabilities.

Rain attenuation is the dominant propagation impairment at frequencies above about 10 GHz. In addition, other impairments such as gaseous absorption, cloud attenuation, melting layer attenuation, and tropospheric refractive effects becomes increasingly important with increasing operating frequency. A number of prediction models are available for the estimation of individual components [1]-[4]. However, methodologies that attempt to combine them in a cohesive manner are not widely available. This is partly due to the paucity of reliable measured data required to compare and verify such approaches. The available measured data can be largely grouped into beacon measurements and radiometric observations. In beacon measurements, the strength of a satellite-borne beacon signal is monitored on the ground and the variations of the signal level are interpreted as propagation impairments. However, only a relative measure of the propagation impairments can be obtained due to a lack of an absolute calibration of the measurement system and signal variations induced by the hardware associated with the beacon source as well as the receiving equipment on the ground. Most of the available beacon data have been analyzed with reference to clear-sky conditions, and this process essentially removes the bulk of the low-attenuation producing phenomena. Radiometers rely on sky noise temperature variations to estimate propagation impairments. Although the technique provides an absolute measure of the impairment level, only absorptive phenomena due to particulate matter and gases can be measured. In addition, there are several limitations to radiometer observations, including restricted dynamic range and the sensitivity to thermal emissions from regions outside those that affect a satellite link at the same look angle as the radiometer. In order to capture all propagation phenomena a combination of beacon and radiometer measurements are normally required. Some of the more recent data collected using the

INTELSAT system [5], the European Space Agency (ESA) Olympus satellite [6], and the National Aeronautics and Space Administration (NASA) Advanced Communications Technology Satellite (ACTS) [7] are of this type and provide a useful database to enable the evaluation of propagation models which attempt to combine different propagation effects.

In synthesizing an overall propagation impairment prediction procedure both existing and new models were used for individual phenomena. Well established models exist for gaseous absorption and tropospheric scintillations [1]. It has been reported that most of the available rain attenuation prediction models provide an annual average accuracy of the order of 30% [8], a level which is usually not considered acceptable to satellite system designers. The model accuracy reported in [8] is supported by recent testing efforts in the ITU-R [35]. A lower limit to the prediction accuracy for rain attenuation models is set by the natural variability of the rain process itself, which is thought to be around 20% on an annual basis [33].

This paper reports on an effort to devise a rain attenuation prediction procedure that provides an accuracy comparable with the natural variability. In addition, new methodologies for predicting cloud attenuation and low-angle fading were also developed since these phenomena become increasingly important at low elevation angles. Descriptions of individual prediction methods used in constructing the overall model are given in Section 2. The approach taken in combining the individual components to derive the overall attenuation distribution is presented in Section 3. An evaluation of the model was carried out using some of the more recent slant path data that have been collected with beacon/radiometer techniques; results of the evaluation are presented in Section 4.

II. PROPAGATION MODELS

Propagation factors considered for inclusion in the overall prediction procedure are: gaseous absorption, cloud attenuation, melting layer attenuation, rain attenuation, tropospheric scintillations, and low-angle fading. Low-angle fading is a refractive phenomena encountered on very low elevation angle paths (<5°) when the propagation path passes at grazing incidence across a boundary between two air masses of different refractive index, thereby causing focussing and defocussing of the energy as the air/air boundary moves with respect to the path [24]. Other impairments that affect satellite links in the Fixed Satellite Service (FSS) are bulk refractive effects and ionosphere effects. These were not considered for the discussion due to the existence of standard procedures for the

prediction of bulk refractive effects[9] and the fact that the ionosphere does not produce significant signal

degradation at frequencies above about 10 GHz. Prediction procedures used for the selected components are

presented below.

A. Gaseous Absorption

A method for predicting absorption due to atmospheric gases (oxygen and water vapor) is given in ITU-R

Recommendation P.618 [1]. The input parameters required for the calculation include frequency, path elevation

angle, height above mean sea level, and the water vapor density. The calculation procedure is reproduced in Annex

I. The oxygen attenuation is considered a background effect with very little temporal variation; variations in

gaseous absorption arise from changes in the amount of water vapor in the atmosphere. In order to estimate the

distribution of gaseous absorption on an annual basis, the annual distribution of water vapor density is required. It

is generally observed that the water vapor density distribution follows the normal probability law [10]. If a

complete characterization of the distribution is not available an approximate distribution can be constructed using

the annual average water vapor density as the mean value and a quarter of that as the standard deviation.

B. Cloud Attenuation

Several models are available for the prediction of cloud attenuation [11]-[14]. An evaluation of these

models by the authors revealed that they are either poor estimators or the input data required are difficult to obtain

for a general purpose application. A comparison of different cloud models presented in [38] largely confirms this

assertion*.* In view of this, a cloud attenuation model based on available cloud cover data and the average properties

of different cloud types was developed. A cloud cover atlas based on daily visual observations of cloud can be

found in Reference 15. A ten year observation period has been used in constructing the maps. Cloud cover

percentages for different cloud types are given for land areas with a resolution of 5°x5° in longitude and latitude.

The data grid resolution is commensurate with the geographical distribution of the data collecting centers and this

level of resolution is deemed reasonable for the calculation of cloud attenuation. It should be noted that rain zones

[2,10] are employed in the prediction of rain attenuation and the rain zones have much larger geographical extents

compared to the 5°x5° grid used for clouds. Although cloud distributions in adjacent grids do not differ

significantly from each other, marked differences in individual cloud amounts are encountered when latitude separation exceeds about 10°. Four cloud types were selected for the development of the cloud attenuation model, and Table 1 summarizes the average properties of the selected cloud types derived from [39] and [40].

TABLE I

Average Properties of the Four Cloud Types Used in the Cloud Attenuation Model

Cloud Type	Vertical Extent (km) H_c	Horizontal Extent (km) L_c	Water Content (g/m^3) υ
Cumulonimbus	3.0	4.0	1.0
Cumulus	2.0	3.0	0.6
Nimbostratus	0.8	10.0	1.0
Stratus	0.6	10.0	0.4

The model was derived using the average cloud properties together with the assumption that the statistical distribution of cloud attenuation follows the log-normal probability law. This assumption is thought to be reasonable considering that most measured slant-path attenuation data conform to the log-normal distribution. It is also assumed that there is no overlap between the occurrence probabilities of the four cloud types so that the attenuation produced by each cloud type represents a distinct point in the probability distribution.

The annual cumulative contributions of cloud attenuation from the various cloud formations encountered at different heights along a zenith path at a given location are obtained from the annual average total cloud cover, individual cloud cover amounts for the four cloud types, their vertical dimensions, and the specific attenuation. This provides the zenith cloud attenuation distribution, with the distribution being conditioned to the total cloud cover.

The cloud attenuation model requires four steps as set out below.

Step 1

The specific attenuation for each of the four cloud types is obtained. These can be related to the cloud water content using the Rayleigh approximation for small water droplets [16]:

$$\alpha_{ci} = 0.4343 \left(\frac{3\pi\upsilon}{32\lambda\rho}\right) Im\left(\frac{1-\varepsilon}{2+\varepsilon}\right) \qquad \text{(dB/km)} \qquad (1)$$

where υ - cloud liquid water content (g/m^3)

λ - wavelength (m)

ρ - density of water (g/cm^3)

ε - complex dielectric constant of water

Im - imaginary part of a complex number

and i is 1 to 4 for the four cloud types.

The above relationship is temperature dependent through the complex dielectric constant and the density of water. However, the sensitivity to temperature is a second order effect and the specific attenuation calculated at 0°C is used in the model.

Step 2

Total zenith attenuation A_{ci} for each of the cloud types (i=1 to 4) is given by the product of the specific attenuation and the vertical extent, namely:

$$A_{ci} = 1/3\ \alpha_{ci}\ H_{ci} \qquad (2)$$

For elevation angles other than zenith, the attenuation through each cloud type is calculated assuming the cloud shape to be a vertical cylinder having the horizontal and vertical dimensions (H_c and L_c) shown in Table 1.

Step 3.

The four cloud types when arranged in rank order of attenuation provide four points on the conditional cloud attenuation distribution curve, A_c, which has the following form:

$$P(A> A_c) = \frac{P_o}{2} erfc\left(\frac{\ln A - \ln \overline{A}_c}{\sqrt{2}\ \sigma_c}\right) \qquad (3)$$

where P is the probability of cloud attenuation A_c not exceeding A, P_o is the probability of cloud attenuation being present, erfc denotes the complementary error function, $\overline{A}_c$ is the mean value of A_c and σ_c is the standard deviation of A_c. The total cloud cover provides the conditional probability for the cloud attenuation distribution.

Step 4

With the five points selected above, the best fit log-normal relationship for the cloud attenuation distribution is obtained using linear regression analysis.

The model is fairly simple and assumes that different parts of the cumulative cloud attenuation distribution, A_c, are accounted for by a single cloud type. This is not strictly true since cloud properties vary widely and the same attenuation level can be expected from more than one cloud type. In addition, different cloud types can be present simultaneously at a variety of heights. However, the available data do not permit the development of a model which can account for the attenuation distribution of each individual cloud type.

In order to combine the attenuation contribution of clouds into a comprehensive prediction procedure, it is necessary to define the end-points of the cumulative distribution of path attenuation due to clouds. The minimum-attenuation end-point will be defined by the onset of "clear-sky" conditions, when no clouds are present; the maximum-attenuation end-point will be set at the point when light rainfall exists in the path. To obtain the percentage-time boundary between clear-sky conditions and clouds being present, average total cloud cover data were used: this will define the high percentage time end of the cloud attenuation distribution. To obtain the low percentage time end of the cloud attenuation distribution, the point where rain and melting layer attenuation merge with cloud attenuation is used. The latter point, where rain, melting layer, and cloud effects merge, is not a well defined boundary and will depend on both the geographic location and the elevation angle. This aspect of cloud attenuation modeling is discussed in section 3 on combining the impairments.

Examples of model predictions compared with direct estimates of cloud attenuation data are shown in Figures 1a and 1b. Data in Fig. 1a are from Darmstadt in Germany [17] where radiometers have been used to estimate cloud attenuation statistics for a period of 12 months. The cloud attenuation estimate for New York, NY, shown in Fig. 1b is based on one year of surface and radiosonde observations. Percentage cloud cover amounts used for the model predictions and the best fit log-normal distribution parameters for the two sites are shown Table 2. It is seen that in both cases good agreement between the model prediction and the direct estimate exist.

TABLE 2

Cloud Parameters for the Predicted Cloud Attenuation Distributions Shown in Figure 1

Parameter	Darmstadt	New York
Percentage of Cumulo Nimbus	2.0	2.3
Percentage of Cumulus	4.0	3.0
Percentage of Nimbostratus	12.0	13.5
Percentage of Stratus	37.3	34.5
Percentage of Total Cloud Cover, P_o	63.3	70.5
$\overline{A}_c$	0.433	0.227
σ_c	0.705	0.956

C. Melting Layer Attenuation

The melting layer is the region around the 0°C isotherm where ice and snow particles from aloft melt to form rain drops. The melting layer thickness, D_m, is of the order of 500 m and a distinct layer such as the radar bright band exists only for relatively low rain rates [18]. Attenuation produced by the melting ice particles can reach significant levels, especially for low-elevation angle links. The specific attenuation in the melting layer, however, is not always significantly larger than that in the rain region underneath it. Rain attenuation modeling, being largely semi-empirical, normally accounts for melting effects for moderate to high rainfall rates (i.e. ≥ 2 mm/h). As such, it is felt that a separate account of the layer is required only for low rain rates. Several models for predicting melting layer effects are available [19]-[21] and the one proposed in Reference 21 was selected for its ease of implementation. Using this model the following relationship between the rain rate, R, and the specific attenuation in the melting layer, α_m, was derived:

$$\alpha_m = aR^b \quad (dB/km) \tag{4}$$

where

$$a = e^{1.58 \ln (f) - 6.23}$$

$$b = e^{0.029 \ln(f) + 0.031}$$

and R is the rain rate in mm/h and f is the frequency in GHz.

The width of the melting layer, D_m, is taken to be 0.5 km and the path length through the melting layer, L_m, is taken to be $L_m = \dfrac{0.5}{\sin\theta}$ (km) where θ is the elevation angle; the path length is restricted to a maximum value of 10 km. Thus, melting layer attenuation, A_m, is given by:

$$A_m = \alpha_m \, L_m \quad \text{(dB)} \qquad\qquad \text{for } L_m \leq 10 \text{ km max.} \qquad\qquad (5)$$

D. Rain Attenuation

   Rain attenuation modeling on satellite paths has been undertaken by many research groups over the last four decades. The models generally fall into two categories: (a) those that attempt to define the physics of the process and model the constituents of storm cells, etc., and (b) those that use empirical approaches with simplified assumptions. Due to the lack of world-wide information on many of the physical inputs needed to provide accurate results using the models of type (a), type (b) models - empirical procedures - have tended to be used most often and with usually the best results. In Working Party 3M of Study Group 3, extensive testing of all of the leading rain attenuation models has been undertaken [35] and the better formulated of the empirical models scored the highest, one of them being the current ITU-R procedure [1].

   The proposed rain attenuation prediction model is somewhat similar to the one recommended by the ITU-R [1] where the rain related input to the model is the rain intensity at the 0.01% probability level. The method was derived on the basis of the log-normal distribution using similarity principles [22]. Both point rain intensity and path attenuation distributions generally conform to the log-normal distribution given by equation (3). Inhomogeniety in rain in the horizontal and vertical directions are accounted for in the prediction. The same procedure applies for both slant paths and terrestrial paths. The method is applicable across the frequency range 4 to 35 GHz and percentage probability range 0.001% to 10%. Input data required for the model and the step-by-step procedure for calculating the attenuation distribution is given below.

   Input data required for the model are:

   • latitude of the earth station - ϕ (deg)

   • altitude of the earth station above the mean sea level - h_s (km)

   • point rainfall rate for 0.01% of an average year - $R_{0.01}$ (mm/hr)

   • percentage exceedance probability for which attenuation is to be calculated - p

- elevation angle - θ (deg)

- frequency - f (GHz)

- polarization angle - ξ (deg)

- effective earth radius - R_e = 8500 km

Step 1

Freezing height during rain, h_{fr} (km), is calculated from the absolute value of station latitude, ϕ (degrees),

as:

$$h_{fr} = 5.0 \qquad\qquad\qquad \text{for } 0° \leq \phi < 23°$$

$$(6)$$

$$h_{fr} = 5.0 - 0.075 (\phi - 23) \quad \text{for } \phi \geq 23°$$

Step 2

The slant-path length, L_S, below the freezing height is obtained from

$$L_S = (h_{fr} - h_S) / \sin\theta \qquad\qquad \text{(km)} \qquad\qquad (7)$$

where θ is the elevation angle and h_S is the station height in km. For elevation angles less than 5°, a more accurate

path length estimate can be made using:

$$L_S = \frac{2(h_{fr} - h_S)}{\left[\sin^2\theta + \dfrac{2(h_{fr} - h_S)}{R_e}\right]^{1/2} + \sin\theta} \qquad \text{(km)} \qquad\qquad (8)$$

Step 3

The horizontal projection, L_g, of the slant path length is found from:

$$L_g = L_S \cos\theta \qquad\qquad \text{(km)} \qquad\qquad (9)$$

Step 4

Obtain the rain intensity, $R_{0.01}$ (mm/hr), exceeded for 0.01% of an average year, and calculate the specific

attenuation, γ (dB/km), using widely published frequency and polarization dependent coefficients k and α [9],[31]

:

$$\gamma = k (R_{0.01})^{\alpha} \quad \text{(dB/km)} \qquad\qquad (10)$$

Step 5

Calculate the horizontal path adjustment factor, $rh_{0.01}$, for 0.01% of the time:

$$rh_{0.01} = \frac{1}{1 + 0.78\sqrt{\dfrac{L_g\gamma}{f}} - 0.38\,[1 - \exp(-2L_g)]} \tag{11}$$

where f is frequency in GHz.

Step 6

Calculate the adjusted rainy path length, L_r (km), through rain:

$$L_r = \frac{L_g\,rh_{0.01}}{\cos\theta} \qquad\qquad \text{for } z > \theta$$

$$\tag{12}$$

$$L_r = \frac{h_{fr}-h_s}{\sin\theta} \qquad\qquad \text{for } \zeta \leq \theta$$

where $\zeta = \tan^{-1}\!\left(\dfrac{h_{fr}-h_s}{L_g\,rh_{0.01}}\right)$

Step 7

Calculate the vertical adjustment factor, $rv_{0.01}$, for 0.01% of the time:

$$rv_{0.01} = \frac{1}{1 + \sqrt{\sin\theta}\left[31\,(1- e^{-\theta/[1+\chi]})\dfrac{\sqrt{L_r\gamma}}{f^2} - 0.45\right]} \tag{13}$$

where $\chi = 36 - |\phi|$ for $|\phi| < 36°$

$\chi = 0$ for $|\phi| \geq 36°$

Step 8

The effective path length through rain, L_e (km), is given by:

$$L_e = L_r\,rv_{0.01} \qquad\qquad \text{(km)} \tag{14}$$

Step 9

The attenuation exceeded for 0.01% of an average year may then be obtained from:

$$A_{0.01} = \gamma\,L_e \qquad\qquad \text{(dB)} \tag{15}$$

Step 10

The attenuation to be exceeded for other percentages of an average year, in the range 0.001% to 10.0%, may

be estimated from the attenuation to be exceeded for 0.01% for an average year by using:

$$A_p = A_{0.01} \left(\frac{p}{0.01}\right)^{-[0.655 + 0.033 \ln p - 0.045 \ln A_{0.01} - z \sin\theta (1-p)]} \qquad (16)$$

where p is the percentage probability of interest and z is given by:

For $p \geq 1\%$ $z = 0$

for $p < 1\%$

     $z = 0$ for $|\phi| \geq 36°$

     $z = -0.005 (|\phi| - 36)$ for $\theta \geq 25°$ and $|\phi| < 36°$

     $z = -0.005 (|\phi| - 36) + 1.8 - 4.25 \sin\theta$ for $\theta < 25°$ and $|\phi| < 36°$

The above procedure was tested by the ITU-R and found to be the most accurate overall of all models tested [35].

E. Tropospheric Scintillations

A procedure for predicting tropospheric scintillation is given in the ITU-R Recommendation 618 [1]; this is reproduced in Annex II. The key input parameters for the model are: frequency, elevation angle, antenna diameter, average temperature and average relative humidity. It first calculates the standard deviation of the signal amplitude fluctuations, σ_χ, from which the scintillation distribution is constructed. The model is semi-empirical and has been found in testing by ITU-R Study Group 3 to replicate measured results very well at elevation angles above about 4° (see, for example, [36]).

F. Low-angle Fading

In still air, the atmosphere assumes a stratified form with layers of generally decreasing refractive index lying one above the other. Slight horizontal wind movement will cause these layers to fold, rather like the strata of the Earth under tectonic stress, such that the boundary between layers of different refractive index can be inclined a few degrees to the horizontal. This slight change in angle has no effect on satellite links with elevation angles well above 10°. At elevation angles below 10°, and particularly below 5°, the signal path to or from the satellite may be at grazing incidence to the tilted air/air refractive index boundary. Changes in position of the refractive index boundary with respect to the signal path, brought about by relative movement of the atmospheric layers and the satellite path, can lead to large changes in energy levels at the ends of the signal path. These changes are due to large scale refractive irregularities across the layer boundary and thus have a minimal dependence on radio frequency,

unlike tropospheric scintillation which is due to small scale refractive index variations and which therefore has a

strong frequency dependence [1].

The ITU-R tropospheric scintillation model performs quite well for elevation angles down to about 5°.

Below this elevation angle, low-angle fading begins to appear in measured cumulative statistics. After an

investigation of available scintillation data for elevation angles below 5°, the ITU model was extended below 5°

elevation angles in this new approach by supplementing the tropospheric scintillation fading with additional fading

due to low-angle effects. The extension to the scintillation model in this paper modifies the ITU-R tropospheric

scintillation standard deviation,

σ_χ, and takes effect only at elevation angles below 5°. The modified standard deviation σ_t for deriving the fading

distribution is given by:

$$\sigma_t = \sigma_\chi + \sigma_0 \, (e^{a(5-\theta)} - 1.0) \qquad\qquad (0° < \theta < 5°) \qquad\qquad (17)$$

where σ_0 is the scintillation standard deviation at a frequency of 4 GHz and an antenna diameter of 4 m, and a is an

empirical constant equal to 0.11.   The σ_0 term accounts for low-angle fading which is essentially frequency

independent. It was derived using experimental fading data from two experiments; one in Clarksburg, MD [23],

and the other in Ottawa, Canada [24]. Both experiments used antennas with diameters close to 4 m.

Predictions made with the above equation are compared with measured results in Figure 2. The

discrepancy between the measured and the predicted fades appears to compare well with potential errors involved in

the measurements of signal scintillations and low-angle fading. It should be noted that unlike in the ITU

scintillation model, σ_t applies only to the fading part of the distribution. The tropospheric scintillation model [1]

has been recommended for use between 4 and 20 GHz, but recent Olympus and ACTS measurements have shown it

to be accurate in predicting scintillation effects up to about 30 GHz. The low-angle fading model presented here

included the ITU-R tropospheric scintillation model and so should be applicable up to at least 30 GHz.

III. COMBINING IMPAIRMENTS

All the propagation impairments discussed in previous sections originate in the lower troposphere and their respective sources are highly interdependent. Some examples are: cumulus clouds can produce both attenuation and scintillations; the melting layer is associated with low-intensity rain; and gaseous absorption increases during rain due the increased water vapor content in the atmosphere. As a result, a procedure for combining the different impairments to produce an overall cumulative fade distribution is not directly evident. This is compounded by the fact that most impairment prediction models are semi-empirical in nature due to an incomplete understanding of the physical mechanisms as well as the lack of an adequate characterization of the various sources producing the impairments. Methodologies available for combining impairments generally limit themselves to combining only the absorptive and non-absorptive components [1,37].

Several approaches were considered for combining the individual attenuation contributions to produce the overall attenuation distribution. These were: direct addition on an equi-probable basis, root-sum-square addition on an equi-probable basis, equi-probable weighted addition, and statistical interpolation. A combination of these approaches was used for the various impairment phenomena. Two main areas of uncertainty were encountered: (1) how to combine the individual attenuation contributions and, as fundamental, (2) how to approach the transition region between clear-air and precipitation.

For topic (1), several approaches were considered for combining the individual contributions. These were: direct addition on an equiprobable basis; a root-summed-squared addition on an equiprobable basis; an equiprobable weighted addition; and statistical interpolation. A combination of these approaches was eventually used as will be shown later in this section. For topic (2) an empirical approach to combining impairments in this region was taken by identifying possible approaches and checking them against the measured distributions. To this end, statistical interpolation and equi-probable weighted addition were considered. Measured data normally show that the attenuation distribution is continuous, with no break-point between the clear-air region and the precipitation region. On this basis it was thought appropriate to divide the absorptive part of the overall attenuation distribution into two distinct regions, viz. clear-air and precipitation , with the region in between filled in with interpolated values. This worked well at frequencies below 10 GHz since the attenuation produced by low precipitation levels was comparable to those produced by clouds and a smooth transition between the clear-sky and precipitation regions resulted. Due

to the relatively low levels of attenuation expected at frequencies of less than 10 GHz, a fixed set of boundaries were selected. These were:

• the precipitation region was defined by percent probabilities < 0.5%

• the clear-air region was defined by percent probabilities > 10%

Attenuation statistics are assumed to follow a log-normal distribution and the attenuation in the transition region between the precipitation region and the clear-air region derived using log-normal interpolation between the attenuation values at 0.5% and 10%.

For frequencies above 10 GHz, a different approach was found to be necessary. This combined impairments using a weighted sum of absorptive components for probability levels between τ_1% and τ_2%; τ_1 is a variable dependent on the rain climate and τ_2 is a function of the elevation angle. Above the τ_2% level, the impairments are entirely due to clear-air effects and below τ_1% mainly rain attenuation and gaseous absorption contribute to the absorptive component. The τ_1 level is set by the upper limit of rain rate for which the melting layer attenuation model is considered valid (i.e. $R \leq 2$ mm/h). The resulting distribution for the absorptive components can now be added to the scintillation contributions on a root-sum-squared basis [1]. The root-sum addition between absorptive and non-absorptive components appears to produce adequate results that compare well with measured data.

For the combination process, the following parameters are used.

$A_x(p)$ is the attenuation exceeded for p percent of time with

A_t - total attenuation

A_a - absorptive component

A_s - refractive component

A_r - rain attenuation

A_g - gaseous absorption

A_c - cloud attenuation

A_m - melting layer attenuation

$A_{cm} = \sqrt{A_c^2 + A_m^2}$ - cloud and melting layer attenuation

A_{rcm} - combined attenuation from rain, clouds, and melting layer

f - frequency

θ - elevation angle

The attenuation distribution construction for the probability range between 0.001% and 50% is carried out as follows:

$$A_t(p) = \sqrt{A_a(p)^2 + A_s(p)^2} \qquad\qquad (18)$$

$$A_a(p) = A_{rcm}(p) + A_g(p) \qquad\qquad (19)$$

$$A_{rcm}(p) = A_{cm}(p) + A_r(p) \qquad\qquad (20)$$

$$A_{cm}(p) = \sqrt{A_c(p)^2 + A_m(p)^2} \qquad\qquad (21)$$

For 4 GHz $\leq$ f $\leq$ 10 GHz,

$$A_{rcm}(p) = I_{lnm}(A_r(0.5\%), A_{cm}(10\%)) \qquad\qquad (22)$$

where I_{lnm} stands for the log-normal interpolation between the values predicted at the 0.5% and 10% levels. The log-normal form is as shown in section II B.

For 10 GHz < f < 35 GHz,

$$A_{rcm}(p) = \frac{\tau_2-p}{\tau_2-\tau_1} A_r(p) + \frac{p-\tau_1}{\tau_2-\tau_1} A_{cm}(p) \qquad \tau_1\% \leq p \leq \tau_2\% \quad (23)$$

with

$$\tau_1 = \text{larger of 1\% and } P_{R2}$$

where P_{R2} is the percentage probability of rain rate exceeding 2 mm/hr.

$$\tau_2 = 10 \qquad\qquad\qquad\qquad \text{for } \theta \leq 10°$$

$$\tau_2 = 5 \qquad\qquad\qquad\qquad \text{for } \theta \geq 30°$$

$$\tau_2 = 10 - (\theta-10)/4 \qquad\qquad \text{for } 10° < \theta < 30°$$

IV. MODEL EVALUATION

Evaluation of the overall propagation model described in the previous sections requires reliable measured data that include all pertinent propagation effects. Slant path attenuation data from several hundred links have been compiled into a data bank by the ITU [25]. The bulk of the measured data in the data bank pertains to rain attenuation only, and therefore, cannot be used for evaluating the complete model. However, data from several recent Ku- and Ka-band experiments report attenuation distributions that include most of the impairments and these

are used for the model evaluation; Table 3 gives key parameters of the data sets used for the comparison [6], [25]-[29].

The proposed rain attenuation model requires rain intensity, with an integration time of the order of one minute, exceeded for 0.01% ($R_{0.01}$) as the main input parameter. This parameter can be obtained from a rain model or measured rain intensity data. Since measured rain intensity data are not generally available, recourse must be made to a rain model; Some of the available options are:

- conversion of daily or hourly rain intensity to one minute rain intensity

- rain zone classification of the ITU-R [10]

- Crane global rain model [2]

- Rice-Holmberg rain model [30]

Rain zone models such as the ITU-R and Crane global model embody broader climatic features of widely separated regions. As such, they tend to be rather coarse and may not always be appropriate for obtaining site specific rain intensity data. Conversion of long integration time rain intensity to short integration time rain rates is more direct and can be made site specific using widely available rainfall data from meteorological stations. The Rice-Holmberg (R-H) model requires the average annual accumulation of rainfall and the fraction of this rain arising from thunderstorm activity as input parameters. The model provides one-minute averaged estimates of point rain rate R (mm/h) exceeded for a particular percentage of an average year, P, using the equation:

$$P(r > R) = \frac{M}{87.66} \{ 0.03\beta \, e^{-0.03R} + 0.2 \, (1 - \beta) \, [e^{-0.258R} + 1.86 \, e^{-1.63R}]\} \qquad (24)$$

where

M - average annual accumulation of rainfall (mm)

β - thunderstorm component of M given by [32]:

$\beta = \beta_0 \, [0.25 + 2 \, e^{-0.35 \, (1 + 0.125M)/U}]$

$\beta_0 = 0.03 + 0.97 \, e^{-5 \, \exp(-0.004M_m)}$

where U is the average number of thunderstorm days expected during an average year and M_m is the highest monthly precipitation observed in 30 consecutive years.

The required input data can be obtained from meteorological data sources and regional maps. In addition, they are easier to manipulate than the long integration time rain intensity data. Although the R-H model has been developed largely on the basis of rainfall measurements made in the US, it has been found to be applicable to other parts of the world as well. In light of this, the Rice-Holmberg model was selected to obtain the $R_{0.01}$ values for the rain attenuation calculation. The M and β values for the selected experiment locations are also shown in Table 3. In addition, the Table includes the measured value of $R_{0.01}$ whenever they are available. It can be seen that the agreement between the predicted and measured $R_{0.01}$ values is reasonable. However, consideration to the following must be given when comparing the data:

• most measured rain intensity data shown in Table 3 pertain to a measurement period of one or two years. To obtain stable statistics, a measurement period in excess of five years is usually recommended. Year-to-year variability of rain intensity at a given site can be as much as 30%.

• the thunderstorm factor is an empirically derived parameter based on the number of average thunderstorm days in a year and the maximum monthly rainfall. When these parameters are not available, a less accurate estimate can be made using regional maps of β [32], [33].

The measurement sites listed in Table 3 report total attenuation in some form allowing the model to be compared at probability levels well in excess of 1%. However, not all model components could be included for all sites. Some sites report beacon attenuation data that have been low-pass filtered to remove scintillation effects. In the ensuing comparison the most appropriate impairment components were used in making the predictions.

Comparisons are based on the percentage prediction error defined as:

$$e_i = \frac{A_{pi} - A_{mi}}{A_{mi}} \times 100 \qquad\qquad (25)$$

where A_p is the predicted attenuation and A_m is the measured attenuation, both in dB, and i represents the percent probability level at which the prediction error is estimated. The RMS error is used as the metric to judge the overall fit of the prediction with the measurement, and is given by:

$$e_{rms} = \sqrt{\langle e_i^2 \rangle} \qquad\qquad (26)$$

where <> denotes averaging.

The percent probability levels used for the comparison range from 10%, to 0.001% with four points in each decade of probability (1, 2, 3, and 5). Figures 3 through 14 show comparisons between measured and predicted

attenuation distributions for sites reporting Ka-band measurements. Results of the comparison are given in Table 3.

Out of the 30 links used for the test, 18 produced RMS errors of less than 20%. The average RMS error was

19.5%. One of the links (12.5 GHz at Blacksburg) produced a rather large RMS error of 45%, mainly due to the

relatively high value of the $R_{0.01}$ predicted by the R-H model in comparison with the long-term measured value.

The observation period associated with most of the links is less than two years and part of the prediction error can

be attributed to the annual variability of attenuation. In most cases the errors are comparable to the year-to-year

variability associated with path attenuation, and it can be concluded that the prediction procedure is in reasonable

agreement with the measured data. In recent testing of eleven rain attenuation prediction models [34], the modified

rain attenuation procedure proposed in this paper was found to be the best on average.

V. CONCLUSIONS

A procedure suitable for the prediction of propagation impairments along earth-satellite paths is described.

The method can be used to predict individual impairments as well as their combined effects at frequencies between 4

GHz and 35 GHz although the best accuracy will be found between 10 and 30 GHz. Based on the limited

comparisons presented in Section 4, the method appears to be able to predict total path attenuation with an overall

error of less than 20%. The method predicts the long-term average attenuation values for a given link and the

comparisons were not always made with long-term observations. The year-to-year variability of attenuation on a

given link is of the order of 20% [8] and the prediction accuracy compares well with this value.

The dominant propagation impairment at frequencies above 10 GHz is rain attenuation. The prediction of

rain attenuation requires either measured rain data or a fairly representative rain model to obtain the 0.01% rain rate.

The model comparisons presented in Section 4 were made using the Rice-Holmberg rain model and the relatively

low levels of the prediction error points to the usefulness of this rain model for propagation impairment predictions.

The proposed rain attenuation model can be used for terrestrial paths as well (i.e. for $\theta = 0°$). This feature is

currently a requirement in the ITU-R prediction procedure for rain attenuation. Comparison of the model proposed

here with the terrestrial rain attenuation database in the ITU-R data bank [25] using measured rain intensity data

given in the data bank produced an average RMS prediction error of 23%.

Available measured data appear to validate the cloud attenuation model presented. Cloud attenuation is limited to less than about 1.5 dB at the frequencies used for the model evaluation. The available cloud cover data are rather coarse and a more refined model based on long-term observations of atmospheric profiles of water vapor, pressure, and temperature may be more appropriate for the prediction of cloud attenuation at frequencies higher than about 35 GHz. The procedure outlined in [37] may help to improve this aspect.

The melting layer can play a significant role under low elevation angle conditions. The proposed model is applicable only when a distinct melting layer is present, such as under stratiform rains of low intensity. When a distinct melting layer is not present the specific attenuation in the melting region appears to be comparable to that in the rain region.

The model provides predictions across the probability range of 0.001% to 50%. This range is thought to be adequate for most telecommunication system design purposes. Use of the model outside the specified range is not recommended since all factors required for a complete description of the cumulative distribution are not included in the model.

ACKNOWLEDGMENT

ANNEX I

CALCULATION OF GASEOUS ABSORPTION

Gaseous absorption is calculated as the sum of water vapor absorption and Oxygen absorption [1].

The procedure described below applies to frequencies up to 350 GHz.

The specific attenuation of water vapor, γ_W (dB/km), for a ground level pressure of 1013 hPa and a temperature of 15°C is given by:

$$\gamma_W = \left(0.05 + 0.0021\mu + \frac{3.6}{(f-22.2)^2 + 8.5} + \frac{10.6}{(f-183.3)^2 + 9.0} + \frac{8.9}{(f-325.4)^2 + 26.3}\right) f^2 \mu 10^{-4} \quad \text{(dB/km)} \quad \text{(A1)}$$

where:

f - frequency (GHz)

μ - water vapor density (g/m^3)

The total attenuation due to water vapor is given by:

$$A_W = h_W \gamma_W / \sin\theta \qquad \text{(dB)} \qquad\qquad \text{for } \theta > 10°$$

$$\text{(A2)}$$

$$A_W = \frac{\gamma_W \sqrt{R_e h_W}}{\cos\theta} \; F(\tan\theta \sqrt{R_e/h_W}) \; \text{(dB)} \qquad \text{for } \theta \leq 10°$$

where:

R_e - effective earth radius including refraction (8500 km)

θ - elevation angle

$$F(x) = \frac{1}{0.661x + 0.339\sqrt{x^2 + 5.51}} \qquad\qquad \text{(A3)}$$

h_W - equivalent height of water vapor given by:

$$h_W = h_{Wo}\left(1 + \frac{3}{(f-22.2)^2 + 5} + \frac{5}{(f-183.3)^2 + 6} + \frac{2.5}{(f-325.4)^2 + 4}\right) \; \text{(km)} \qquad \text{(A4)}$$

$h_{Wo} = 1.6$ km (in clear weather outside the absorption regions)

The specific attenuation of oxygen, γ_O (dB/km), is given by:

$$\gamma_O = \left(7.19 \times 10^{-3} + \frac{6.09}{f^2 + 0.227} + \frac{4.81}{(f-57)^2 + 1.5}\right) f^2 \times 10^{-3} \qquad \text{(A5)}$$

where f is frequency in GHz (f < 57 GHz).

The total attenuation is given by:

$$A_O = h_O \gamma_O / \sin\theta \quad \text{(dB)} \qquad\qquad \text{for } \theta > 10°$$

(A6)

$$A_O = \frac{\gamma_O \sqrt{R_e h_O}}{\cos\theta} \; F(\tan\theta \, \sqrt{R_e/h_O} \,) \quad \text{(dB)} \qquad \text{for } \theta \le 10°$$

where:

R_e - effective earth radius including refraction (8500 km)

h_O - equivalent height of the oxygen layer (= 6 km in dry air)

θ - elevation angle

and F(x) is given by (A3).

Gaseous absorption, A_g (dB), due to the two constituent gases (oxygen and water vapor) is given by:

$$A_g = A_W + A_O \quad \text{(dB)} \qquad\qquad\qquad \text{(A7)}$$

ANNEX II

CALCULATION OF TROPOSPHERIC SCINTILLATION

Tropospheric scintillation statistics for elevation angles above 4° are computed using the

scintillation standard deviation averaged over a minimum period of one month [1].

The standard deviation of the scintillation amplitude is given by:

$$\sigma_\chi = \sigma_{\chi ref}\, f^{7/12}\, \frac{g(x)}{(\sin\theta)^{1.2}} \qquad \text{(dB)} \qquad\qquad \text{(A9)}$$

where:

        f - frequency (GHz) $4\,\text{GHz} \le f \le 20\,\text{GHz}$

        θ - elevation angle

$$\sigma_{\chi ref} = 3.6 \times 10^{-3} + 1.0 \times 10^{-4}\, N_{wet} \qquad\qquad \text{(A10)}$$

$$N_{wet} = 3730\, U\, \frac{e_s}{(T+273)^2} \qquad\qquad\qquad \text{(A11)}$$

        U - average relative humidity

        e_s - saturation water vapor pressure (mbar)

        T - temperature (°C)

$$g(x) = \sqrt{3.86(x^2+1)^{11/12}\, \sin[11/6\, \tan^{-1}(1/x)] - 7.08\, x^{5/6}} \qquad \text{(A12)}$$

$$x = 1.22\, h\, D^2 \left(\frac{f}{L}\right) \qquad\qquad\qquad\qquad \text{(A13)}$$

        D - antenna diameter (m)

        h - antenna aperture efficiency

$$L = \frac{2h}{\sqrt{\sin^2\theta + 2.35 \times 10^{-4}} + \sin\theta} \qquad\qquad \text{(A14)}$$

        h = 1000 m - height of the turbulent layer

The fade level A_p (dB), exceeded for p% of the time is given by:

$$A_p = \sigma_\chi\, (-0.061(\log_{10} p)^3 + 0.072(\log_{10} p)^2 - 1.71\log_{10} p + 3.0) \quad \text{(A15)}$$

for $0.01\% \le p < 50\%$

REFERENCES

[1]   ITU Recommendation ITU-R RPN.618-4, 1996

[2]   R. K. Crane, "A two-component rain model for the prediction of

         attenuation statistics," *Radio Science*, vol. 17, pp. 1371-1387, 1982

[3]   M. J. Leitao and P. A. Watson, "Method for prediction of attenuation on   earth-space links

based on radar measurements of the physical structure   of rainfall," *IEE Proc.*, vol. 133 Part F, pp.

429-440, 1986

[4]   C. Capsoni, Fedi, F., and A. Paraboni, "A comprehensive meteorologically

         oriented methodology for the prediction of wave propagation parameters

         in telecommunication applications beyond 10 GHz," *Radio Science*, vol. 22,   pp. 387-393;

1987

[5]   J. E. Allnutt, "INTELSAT propagation experiments: The focus and results   of recent

campaigns," *IEEE Proc.*, vol. 81, pp. 856 - 864, 1993

[6]   P. Baptista (Editor), *Reference Book on Attenuation Measurement and Prediction,* Second

Workshop of the Olympus Propagation Experimenters

         ESA WPP-083, 1994

[7]   F. Davarian (Editor), *Proceedings of NAPEX XIX and APSW VII,* Jet   Propulsion Labs

Publication 95-15, August 1995

[8]   R. K. Crane, "Estimating risk of earth-satellite attenuation prediction,"

         IEEE Proc., vol. 81, pp 905 - 913, 1993

[9]   J. E. Allnutt, *Satellite-to-ground Radiowave Propagation,* London: Peter   Peregrinus Ltd.,

1989

[10]   *Reports of the CCIR: Report 563-4*, CCIR XVllth Plenary Assembly, Dusseldorf, 1990

[11]   D. S. Slobin, "Microwave noise temperature and attenuation of clouds:

         Statistics of these effects at various sites in the United States, Alaska, and

         Hawaii," *Radio Science*, vol. 17, pp. 1443-1454, 1982

[12]   E. A. Altshuler and R. A. Marr, "Cloud attenuation at millimeter   wavelengths," *IEEE*

Trans. Anten. and Prop., vol. 37, pp. 1473-1479, 1989

[13]   F. Dintelmann and G. Ortgies, "A semiempirical model for cloud   attenuation prediction,"

Electron. Lett., vol. 25, pp. 1487-1488, 1989

[14]   E. Salonen, "Prediction models of atmospheric gases and clouds for slant   path attenuation,"

Olympus Utilization Conference, Sevilla, pp. 615 - 622,   1993

[15]   S. G. Warren et al., *Global distribution of total cloud cover and cloud type*

        amounts over land, National Center for Atmospheric Research (NCAR)   Technical Notes,

NCAR/TN-273, October 1986

[16]   R. J. Doviak and D. S. Zrnic, *Doppler Radar and Weather Observations*

        Orlando, Academic Press, 1984

[17]   G. Ortgies, F. Rucker, and F. Dintelman, "Statistics of clear-air attenuation   on satellite links

at 20 and 30 GHz," *Electron. Lett.*, vol. 26, pp. 358 - 360,

        1990

[18]   L. J. Battan, *Radar Observation of the Atmosphere*, Chicago, University of   Chicago Press,

1973

[19]   W. Klassen, *From snowflake to raindrop: Doppler radar observations and*

        simulations of precipitation, Ph.D. dissertation, University of Delft, 1989

[20]   M. M. Z. Kharadly and A. S. V. Choi, "A simplified approach to the evaluation of EMW

propagation characteristics in rain and melting snow,"

        IEEE Trans. Anten. and Prop., vol-36, pp. 282-296, 1988

[21]   A. W. Dissanayake and N. J. McEwan, "Radar and attenuating properties   of rain and bright

band," *IEE Conf. Publ. 169-2*, pp. 125-129, 1978

[22]   A. W. Dissanayake and J. E. Allnutt, "Prediction of rain attenuation in   low-latitude

regions," *URSI Commission F Open Symposium: Wave   propagation and remote sensing*, Ravenscar,

UK, pp. 7.1.1 - 7.1.5,

        June 1992,

[23]   K. T. Lin, A. W. Dissanayake, and C. Cotner, "Propagation impairments   on a very-low

elevation angle C-band satellite link," 1*5th AIAA   International Communications Satellite Conf.*, pp.

932-936, 1994

[24]   J. L. Strickland, R. L. Olsen, and H. L. Werstiuk, "Measurement of low-   angle fading in

the Canadian Arctic," *Ann. Telecom.*, vol 32, pp. 530-535,   1977

[25]   ITU Radiocommunication Sector SG3 Databases, 1993

[26]   Vogel, E. J., Torrence, G. W., Allnutt, J. E.; "Rain fades on low elevation

          angle earth-satellite paths: Comparative assessment of the Austin, Texas,

          11.2 GHz experiment," *IEEE Proc.*, vol. 81, pp. 885 - 896, 1993

[27]   Stutzman, W. L. et al.; Results from Virginia Tech Propagation

          Experiment Using the Olympus Satellite 12, 20, and 30 GHz beacons

          IEEE Trans. Antennas Propagat., vol. 43, pp. 54 - 62, 1995

[28]   F. Davarian Editor, *Presentations of the Eighth ACTS Propagation Studies*

          Workshop, Jet Propulsion Labs Publication D-13157, December 1995

[29]   P. J. L. Maagt, et. al., "Results of 12 GHz Propagation Experiments in

          Indonesia," *Electron. Lett.*, vol. 29, pp. 1988-1990, 1993

[30]   P. L. Rice and N. R. Holmberg, "Cumulative time statistics of surface

          point rainfall rates," *IEEE Trans. Communication*, vol. 21, pp. 1131-1136,   1973

[31]   ITU Recommendation ITU-R RPN.837, 1995

[32]   E. J. Dutton, H. T. Dougherty, and R. F. Martin, "Prediction of European rainfall

          and link performance coefficients at 8 and 30 GHz," US Dept. of Commerce

          Office of Telecommunications, Tech. Report No. ACC-ACO-16-74, 1974

[33]   E. J. Dutton, "Precipitation variability in the USA for microwave terrestrial

          system design," US Dept. of Commerce Office of Telecommunications, OT

          Report 77-134, 1977

[34]   G. Feldhake, "A comparison of 11 rain attenuation models with two years of

          ACTS data from seven sites," *Proceedings of 9th ACTS Propagation Studies*

Workshop (APSW IX), 19-20 November, 1996

[35]   A. Paraboni, "testing of rain attenuation prediction methods against the

measured data contained in the ITU-R data bank," *ITU-R Study Group 3*

Document, SR2-95/6, Geneva, 1995

[36]   D. L. Bryant, "Low elevation angle 11 GHz beacon measurements at Goonhilly

 earth station," *BT Technology*, vol. 10, No. 4, Dec 1992, pp. 68-75

[37]   E. T. Salonen et. al., "Scintillation effects on total fade distribution for earth-

satellite links," *IEEE Trans. Antennas Propagat.,* vol. 44, pp. 23-27, 1996

[38]   G. C. Gerace, E. K. Smith, "A comparison of cloud models," *IEEE Anten. and*

Prop. Magazine, pp. 32-38, October 1990

[39]   B. J. Mason, *The Physics of Clouds,* London, Oxford University Press, 1971

[40]   G. L. Stephens, "Radiation profiles in extended water clouds," *Jnl. Atmospheric*

Sciences, vol. 35, pp. 2111-2122, 1978

Table 3 Comparison of slant path attenuation predictions with measured data. Prediction errors shown as the mean, standard deviation, and RMS value are calculated using the plotted points on the cumulative distribution curves in Figures 3 - 15.

| Site	Latitude	Altitude (m)	Frequency (GHz)	Elevation Angle	Polariza-tion Angle	M (mm)	β	Measured $R_{0.01}$ (mm/hr)	R-H R_{001} (mm/hr)	Mean Error (%)	Std Error (%)	RMS Error (%)
Albertslund, DK [26,6]	55.68	30	11.198 19.77 29.65	4.94 20.64 20.64	45.0 70.4 70.4	600	0.07	25.0	23.6	2.0 -2.8 23.6	15.4 15.6 14.2	15.5 15.9 27.6
Austin, TX[27]	30.3	100	11.198	5.75	45.0	550	0.53	75.0	76.7	10.1	12.3	15.8
Blacksburg, VA [28]	37.23	646	12.5 19.77 29.65	13.93 13.93 13.93	40.8 40.8 40.8	965	0.2	42.0	63.0	18.1 17.2 12.5	41.2 16.6 8.9	45.0 23.8 15.3
Clarksburg, MD [29]	39.2	150	20.18 27.5	38.87 38.87	64.68 64.68	936	0.29	72.0	74.3	-13.7 -8.2	9.5 10.9	16.6 13.7
Eindhoven, NL [6]	51.45	15	12.5 19.77 29.65	26.79 26.79 26.79	71.72 71.72 71.72	770	0.1	31.0	33.3	-31.9 -9.1 25.4	12.1 11.5 16.2	34.1 14.7 30.2
Gometz la Ville, FR [6]	48.67	10	12.5 19.77	30.54	72.42 72.42	600	0.1	68.1	27.6	-1.1 -22.4	14.1 14.6	14.2 26.7
Goonhilly, UK [26]	50.05	100	11.198	3.27	45.0	985	0.07	30.0	31.0	-16.9	15.3	22.9
Kirkkonummi, SF [6]	60.21	60	19.77 29.65	12.68 12.68	68.53 68.53	530	0.1	44.0	25.4	-2.0 1.0	6.4 9.1	6.7 9.2
Lae, PNG [26]	-6.45	50	12.69	72.97	26.68	3302	0.32	107.0	119.6	22.9	25.7	34.4
Montreal, CA [29]	45.6	90	20.18 27.5	31.39 31.39	66.47 66.47	1020	0.11	45.0	44.9	-9.8 -0.5	11.4 11.9	15.0 11.9
Oberpfaffenhofen, DE [6]	48.08	580	19.77	27.53	65.64	900	0.1	37.2	37.9	-0.2	8.8	8.8
Oklahoma, OK [29]	35.23	500	20.18 27.5	48.99 48.99	86.4 86.4	843	0.36	-	78.0	19.9 13.7	19.7 16.0	28.0 21.1
Reston, VA [29]	38.95	150	20.18 27.5	39.1 39.1	64.48 64.48	948	0.28	-	73.0	-5.3 2.3	16.7 16.5	17.5 16.6
Rome, IT [6]	41.87	32	12.5 19.77	32.07 32.07	59.79 59.79	750	0.27	70.0	64.6	-0.8 -6.5	10.4 12.8	10.4 14.4
Spino d'Adda, IT [6]	45.5	84	12.5 19.77	30.54 30.54	64.88 64.88	860	0.15	45.7	49.5	-14.2 -0.2	21.8 9.3	25.9 9.3
Surabaya, IND [30]	-7.3	20	11.198	20.0	45.0	2000	0.7	120.0	125.0	3.1	20.7	21.0
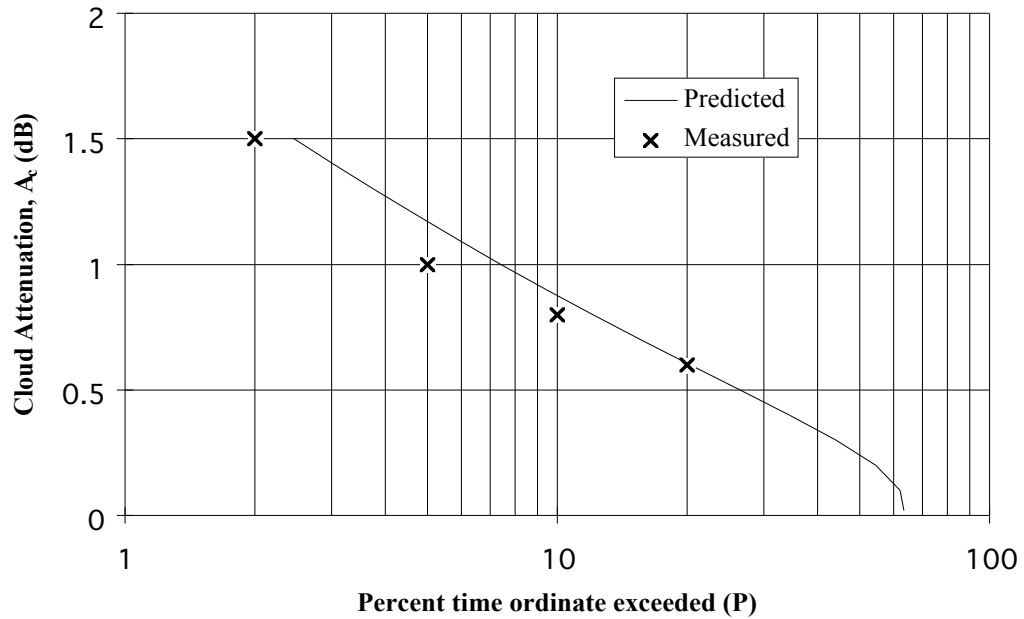
Figure 1a. Comparison of measured and predicted cloud attenuation distributions in Darmstadt, Germany [17]; ⎯ predicted, x: measured; frequency 30 GHz; elevation angle 28 ; cloud amounts use for the prediction are: total cloud cover - 63.3%, stratus - 37.3%, nimbo stratus - 12%, cumulus - 4%, cumulonimbus - 2%.
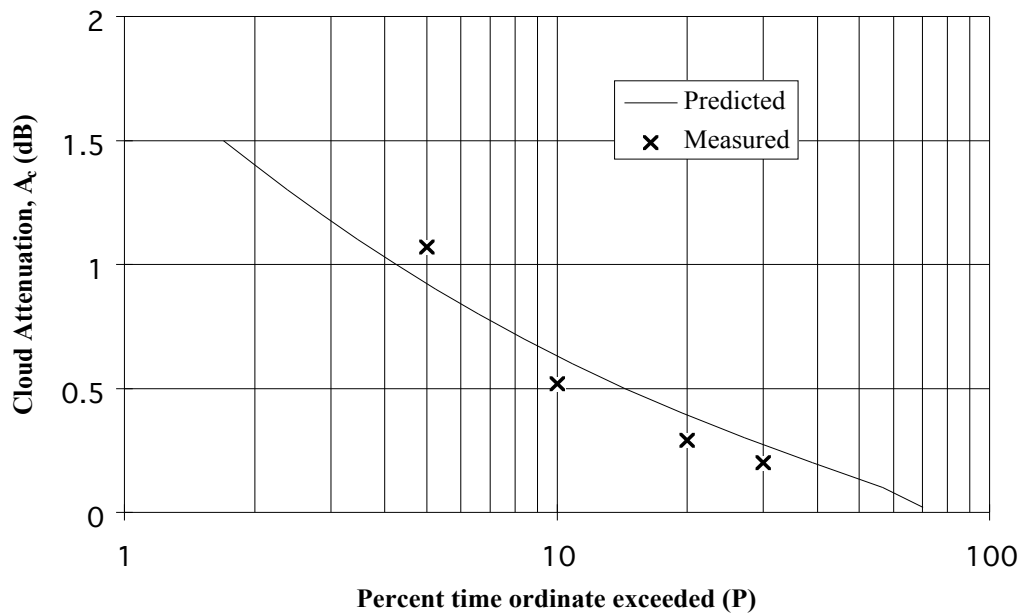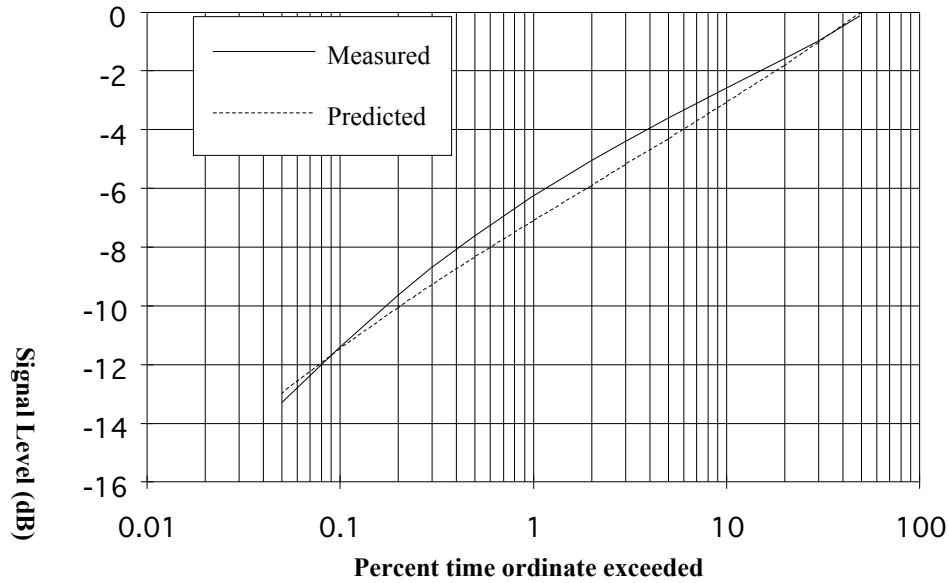

Figure 1b. Cloud attenuation distribution in New York, NY [11]; ⎯ predicted, x: measured; frequency 35 GHz; elevation angle 90 ; cloud amounts use for the prediction are: total cloud cover - 70.5%, stratus - 34.5%, nimbo stratus - 13.5%, cumulus - 3%, cumulonimbus - 2.3%.

Figure 2a. Predicted and measured low-angle fading/tropospheric scintillation distributions of fading on a 2 elevation angle C-band link at Clarksburg, MD [23]; frequency 3.95 GHz; measurement period: 30 days in September 1993.
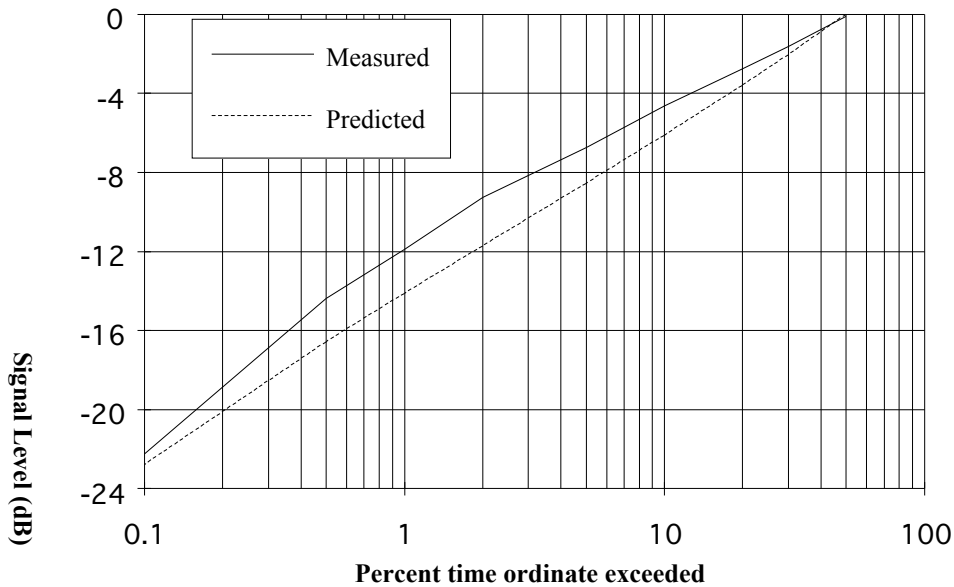
Figure 2b. Predicted and measured low-angle fading/tropospheric scintillation distributions of fading on a 1 elevation angle C-band link at Eureka, Canada [24]; frequency 6 GHz.

Number of points: 14(19.8 GHz), 12(29.7 GHz)
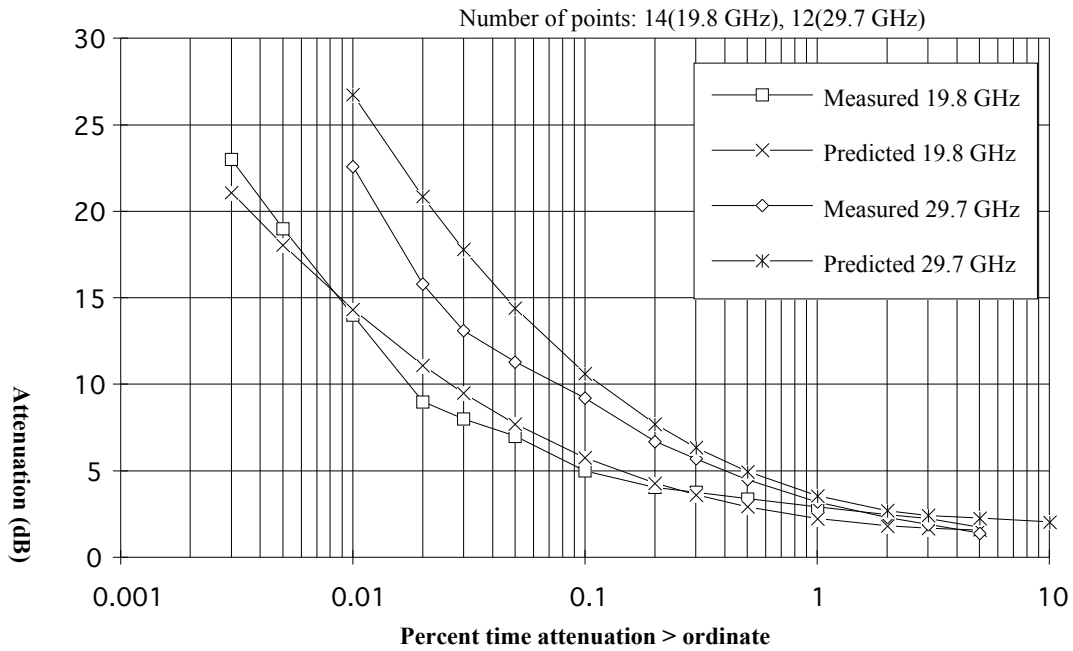
Figure 3. Attenuation distributions at 19.8 and 29.7 GHz at Albertslund, Denmark

Number of points: 13(19.8 GHz), 10(29.7 GHz)
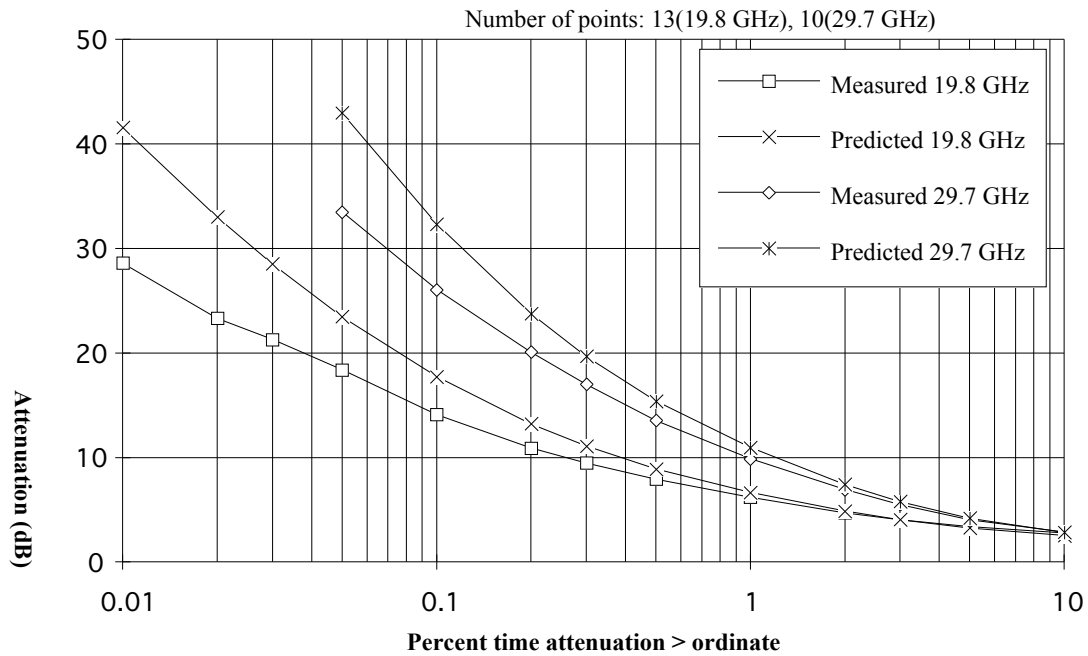
Figure 4. Attenuation distributions at 19.8 and 29.7 GHz at Blacksburg, VA, USA

Number of points: 11(20.2 GHz), 10(27.5 GHz)
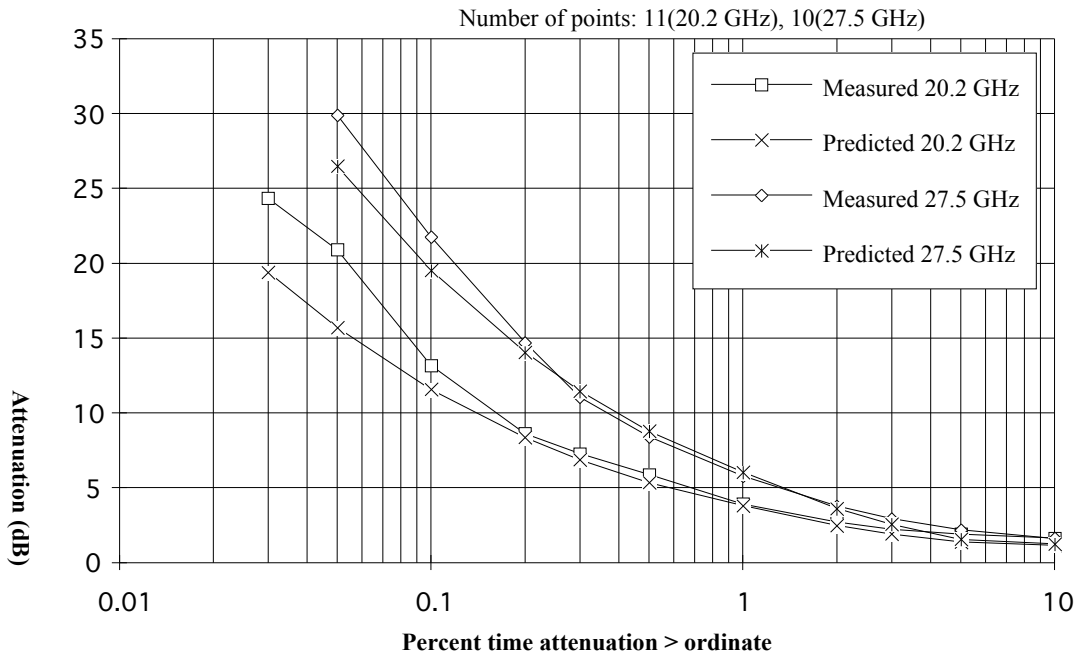
Figure 5. Attenuation distributions at 20.2 and 27.5 GHz at Clarksburg, MD, USA

Number of points: 14(19.8 GHz), 13(29.7 GHz)
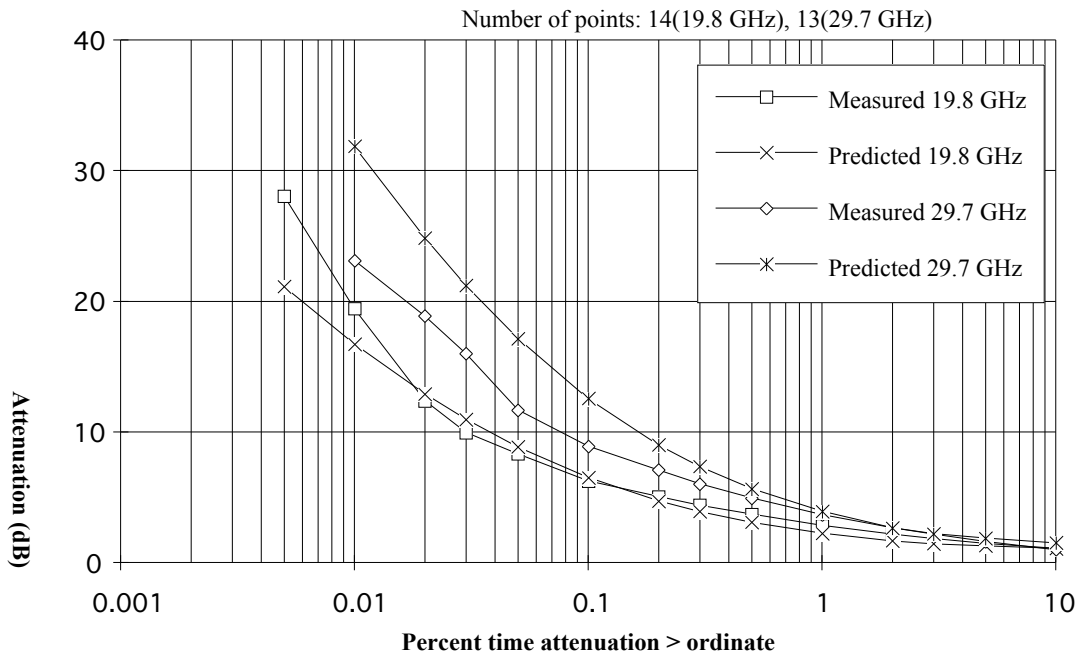
Figure 6. Attenuation distributions at 19.8 and 29.7 GHz at Eindhoven, Netherlands
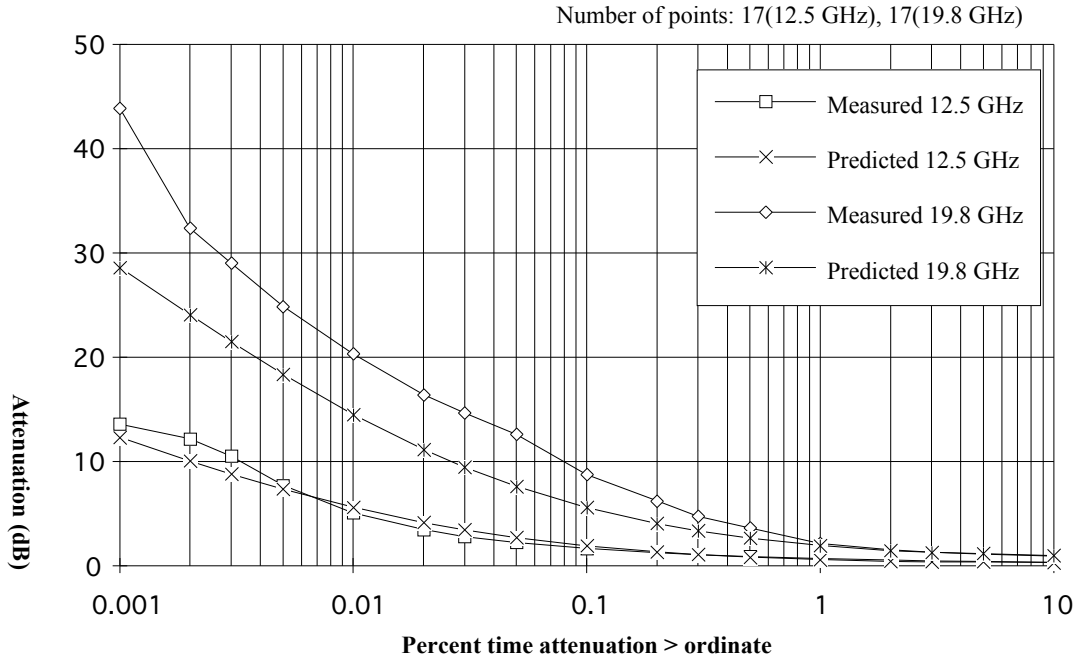
Figure 7. Attenuation distributions at 12.5 and 19.8 GHz at Gometz la Ville, France
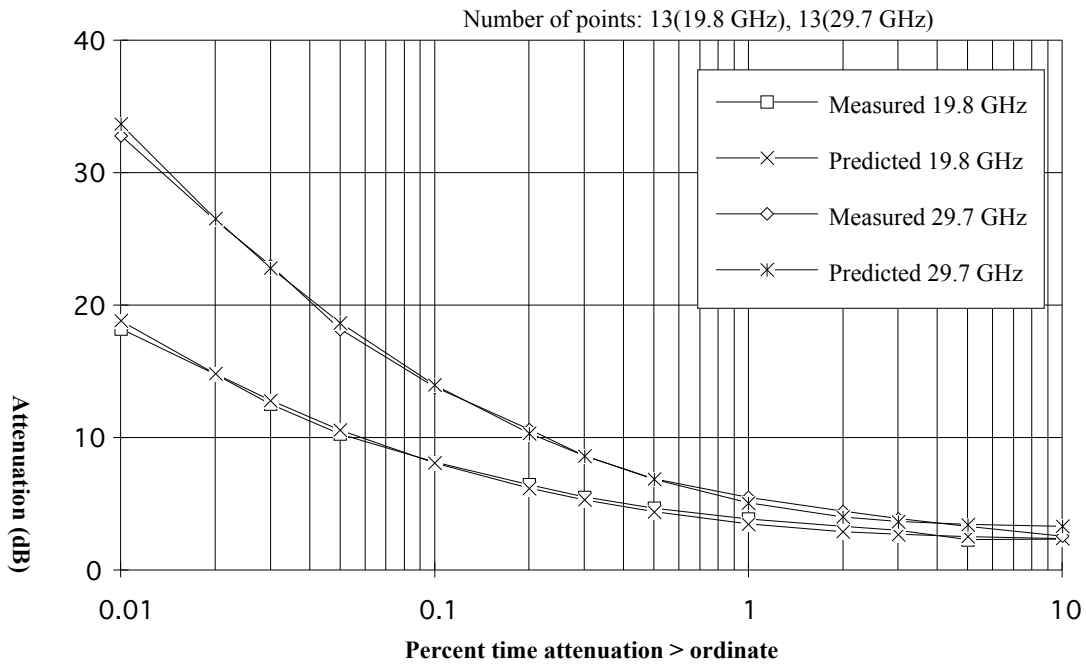
Figure 8. Attenuation distributions at 19.8 and 29.7 GHz at Kirkkonummi, Finland

Number of points: 11(20.2 GHz), 10(27.5 GHz)
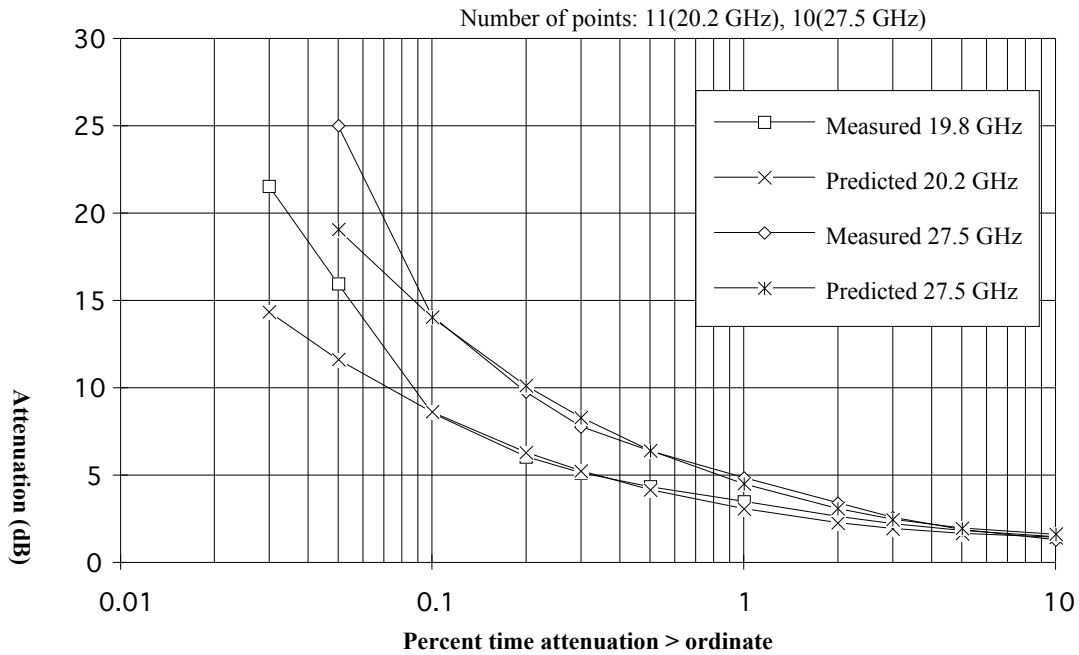
Figure 9. Attenuation distributions at 20.2 and 27.5 GHz at Montreal, Canada

Number of points: 15
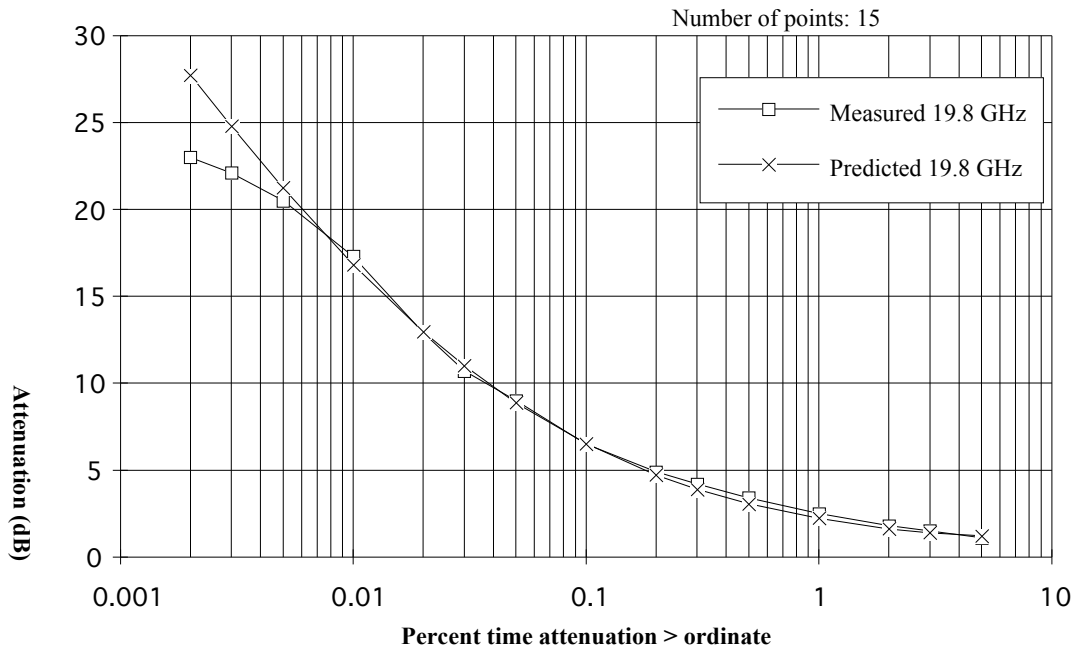
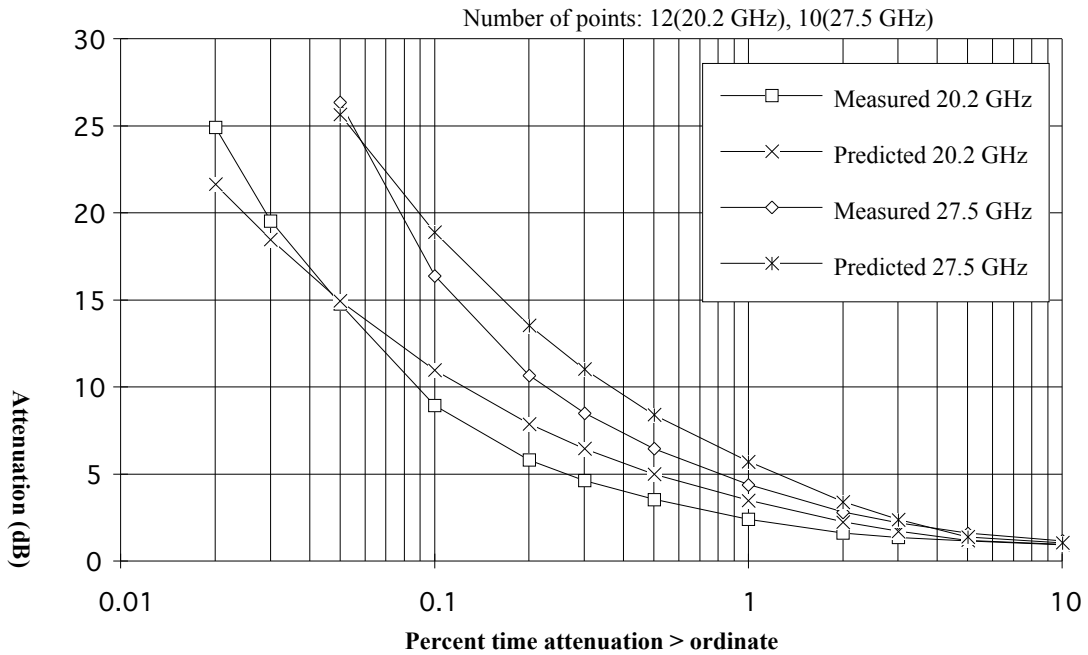Figure 10. Attenuation distributions at 19.8 GHz at Oberpfaffenhofen, Germany

Figure 11. Attenuation distributions at 20.2 and 27.5 GHz at Oklahoma, OK, USA
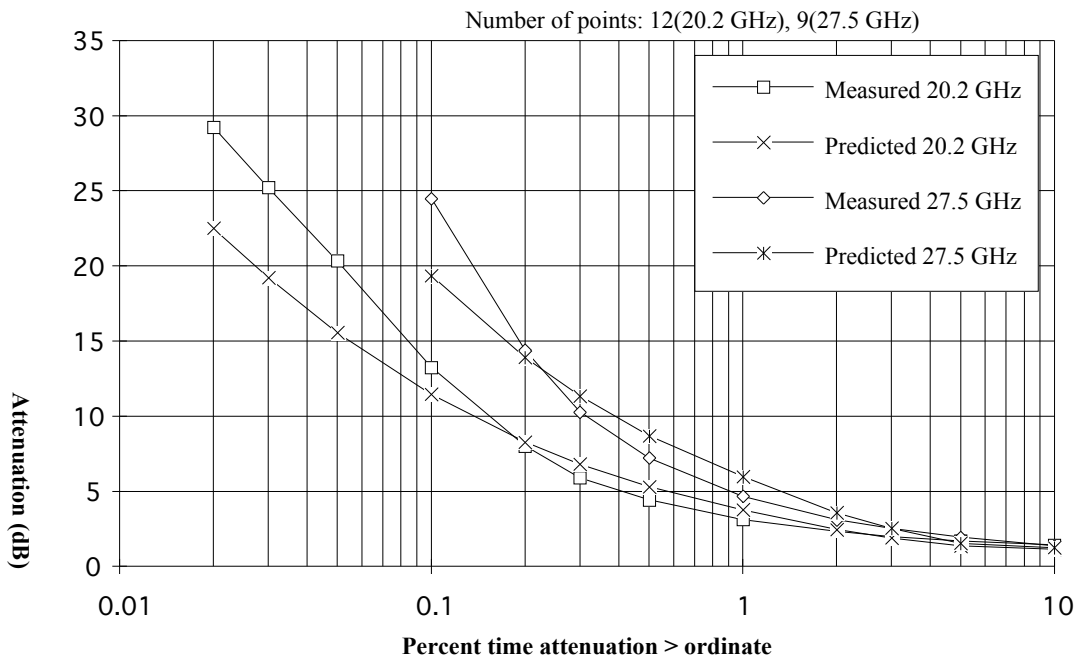

Figure 12. Attenuation distributions at 20.2 and 27.5 GHz at Reston, VA, USA
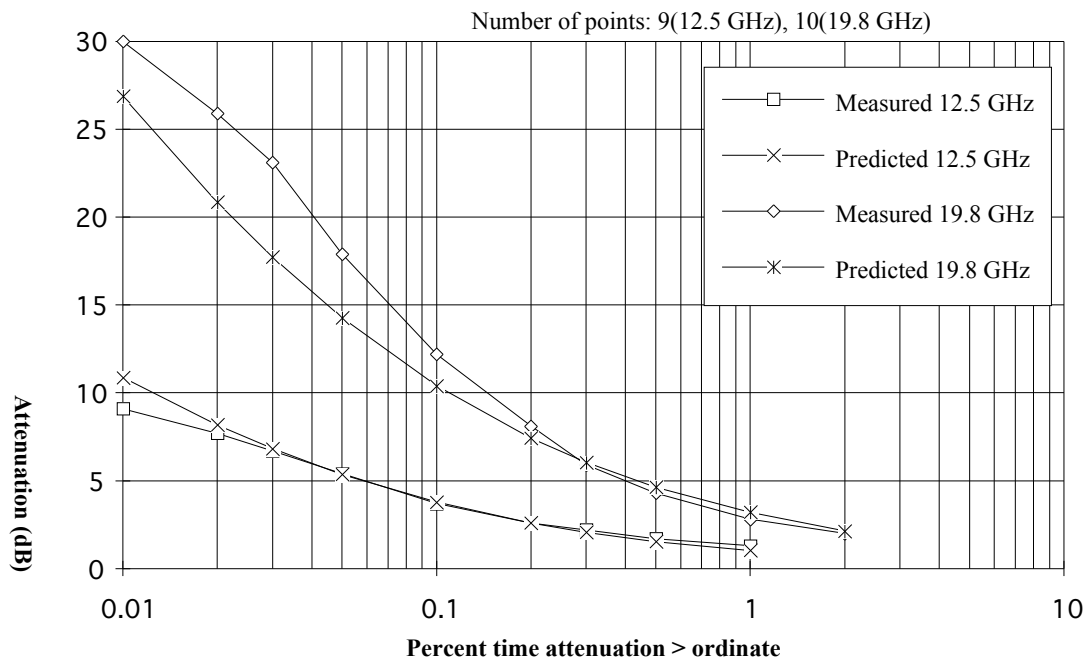
Number of points: 9(12.5 GHz), 10(19.8 GHz)

Figure 13. Attenuation distributions at 12.5 and 19.8 GHz at Rome, Italy

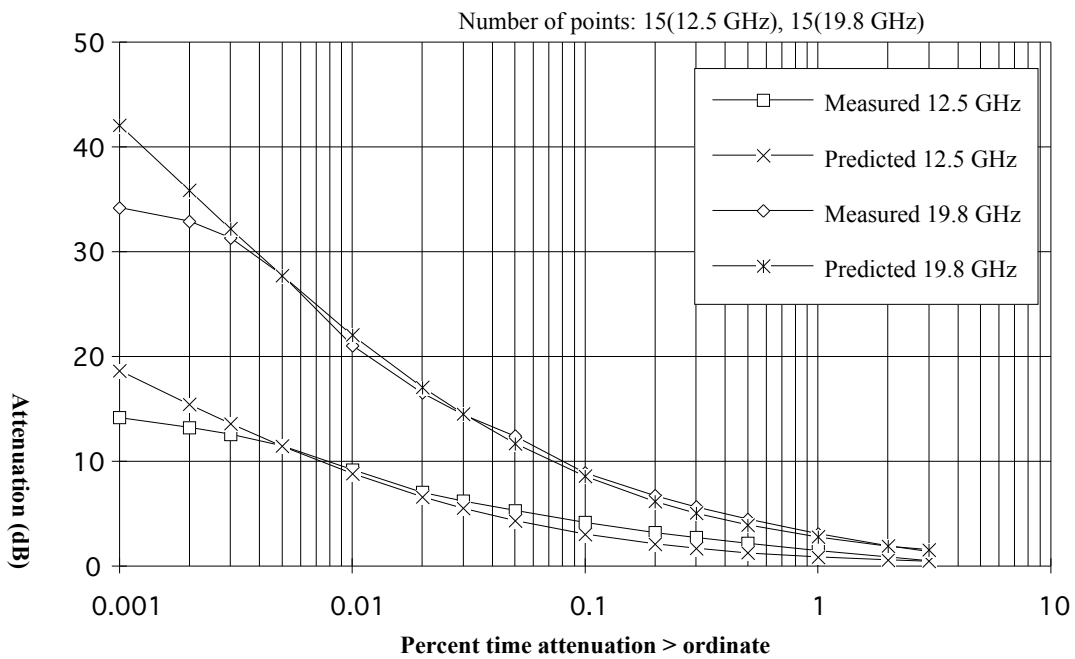Number of points: 15(12.5 GHz), 15(19.8 GHz)

Figure 14. Attenuation distributions at 12.5 and 19.8 GHz at Spino 'd Adda, Italy